



## Aerosol-induced direct radiative forcing effects on terrestrial ecosystem carbon fluxes over China



Wenhai Xue<sup>a</sup>, Jing Zhang<sup>a,\*</sup>, Duoying Ji<sup>a</sup>, Yunfei Che<sup>a,b</sup>, Tianwei Lu<sup>a</sup>, Xiaoqing Deng<sup>a</sup>, Xinyao Li<sup>c</sup>, Yulu Tian<sup>d</sup>, Jing Wei<sup>e,\*\*</sup>

<sup>a</sup> College of Global Change and Earth System Science, Beijing Normal University, Beijing, 100875, China

<sup>b</sup> State Key Laboratory of Severe Weather & Key Laboratory for Cloud Physics, Chinese Academy of Meteorological Sciences, Beijing, 100081, China

<sup>c</sup> Business School, Beijing Normal University, Beijing, 100875, China

<sup>d</sup> Shaanxi Key Laboratory of Earth Surface System and Environmental Carrying Capacity, College of Urban and Environmental Sciences, Northwest University, Xi'an, 710127, China

<sup>e</sup> Department of Chemical and Biochemical Engineering, Iowa Technology Institute, University of Iowa, Iowa City, IA, USA

### ARTICLE INFO

#### Keywords:

Aerosol-induced direct radiative forcing  
Terrestrial ecosystem  
Carbon fluxes  
China  
Global warming

### ABSTRACT

Atmospheric aerosols can change vegetation photosynthesis through the effects of aerosols on radiation, which will affect the peak carbon dioxide emissions and carbon neutrality at global scales. In this study, we quantify the aerosol-induced direct radiation forcing (ADRF) in China from 2001 to 2014 based on the radiation flux simulation used by the Fu-Liou radiation transfer model under with-aerosols and no-aerosols scenarios. Using the radiation simulation results, we modify the atmospheric forcing datasets to drive Community Land Model 4.5 (CLM4.5) to gain the changes in carbon fluxes in China caused by ADRF. The results show that these two models are accurate in estimating radiation ( $R^2 = 0.78\text{--}0.88$ ) and carbon fluxes ( $R^2 = 0.73\text{--}0.75$ ) in China. High levels of ADRFs were captured in China, especially with increasing diffuse fraction, resulting in the diffusing fertilization effect occurring in most areas of China. The ADRF can increase cumulative gross primary productivity (GPP) and total ecosystem respiration (ER) by  $3.20 \text{ gC m}^{-2}$  and  $5.13 \text{ gC m}^{-2}$  per year, respectively. From 2001 to 2014, the diffusing fertilization effects experienced trends of increasing first and then decreasing. However, ADRFs in some regions of China show negative effects on carbon fluxes due to vulnerable vegetation functional types and high aerosol loading. The ADRF will also enable soil temperature decreases and volumetric soil water increases, which is closely related to changes in carbon fluxes. Meanwhile, due to changes in soil water and heat conditions,  $\text{N}_2\text{O}$  and  $\text{CH}_4$  production will also be disturbed, and ADRF increases the global warming potential (GWP) for both greenhouse gases. This phenomenon indicated that atmospheric aerosol pollution control is far-reaching significance for peaking carbon dioxide emissions before 2030.

### 1. Introduction

Since the start of the 21st century, a large amount of aerosols have been released into the atmosphere in China due to the urgent need for economic development (Chan and Yao, 2008; Zhang et al., 2012; Xu et al., 2013; Xue et al., 2021). For human individuals, aerosols, especially fine particles, are closely related to the morbidity of cardiovascular, cerebrovascular, and respiratory diseases (Bartell et al., 2013; Qin et al., 2018; Wei et al., 2021a; Zheng et al., 2015). For the earth system, aerosols also can interact with clouds and solar radiation to affect

climate change and the atmospheric environment (Bellouin et al., 2011; Haywood and Boucher, 2000; Huang et al., 2016, 2020; Yang et al., 2021; Zhang et al., 2010). According to the United Nations Intergovernmental Panel on Climate Change fifth assessment report (IPCC5), the effective radiative forcing caused by atmospheric aerosols is approximately  $-1.9 \sim -0.1 \text{ W m}^{-2}$  (Flato et al., 2013), which greatly affects the assessments of energy at the global scale.

Incipient studies on the relationships between aerosols and radiation are mainly based on ground observations. Mp et al. (1995) found that the solar radiation reaching the ground was reduced due to the rapid

\* Corresponding author.

\*\* Corresponding author.

E-mail addresses: [jingzhang@bnu.edu.cn](mailto:jingzhang@bnu.edu.cn) (J. Zhang), [weijing\\_rs@163.com](mailto:weijing_rs@163.com) (J. Wei).

enhancement of aerosols caused by volcanic eruptions. Gu et al. (2003) found that aerosols can significantly increase the diffuse radiation. Then, aerosol-induced radiation forcing (ARF) had been studied extensively in China due to high aerosol loadings. Li et al. (2010) estimated the mean diurnal cloud-free direct ARF at the top of the atmosphere, surface, and inside atmosphere in China using empirical formulas and surface observations, and found higher intensity of ARF in eastern China with annual mean values of  $-93 \pm 44 \text{ W m}^{-2}$  to  $-79 \pm 39 \text{ W m}^{-2}$  at the surface (Che et al., 2018).

However, because spatiotemporal heterogeneities of ARF (Zhang et al., 2018; Mai et al., 2018), individual-site-scale observations cannot satisfy the analysis for wide-scale regions in China. Fortunately, along with the development of satellite remote sensing and model simulation technologies, many approaches have been proposed to map the radiation, including the radiation transfer mechanism models (Huang et al., 2009), empirical relationship methods (Chen et al., 2019), statistical and machine learning methods (Fan et al., 2019). The radiation transfer mechanism models show a superior performance because they own the synthesized physical-chemistry mechanisms (Lin et al., 2013). In particular, the aerosol-induced direct radiation forcing (ADRF) can be quantified separately, and the ADRF for different aerosol types (e.g., sulfate, dust, and carbonaceous aerosols) can be also calculated (Charlson et al., 1992; Huang et al., 2015; Jia et al., 2018). Overall, ADRFs can alleviate global warming to a certain extent due to the reduction of total radiation (Smith et al., 2016; Yu et al., 2005).

Besides radiation, aerosols can also change the uptake of CO<sub>2</sub> from terrestrial ecosystems to further affect global warming progress (Gao et al., 2018; Shao et al., 2020; Jing et al., 2010). On one hand, aerosols may settle onto vegetation leaves and interference with the absorption of CO<sub>2</sub> and release of oxygen, thereby affecting the normal growth of vegetation (Lee et al., 1981; Yan et al., 2014). On the other hand, aerosols may affect vegetation photosynthesis and respiration by changing solar radiation and meteorological conditions (Greenwald et al., 2006; Zhang et al., 2019). Chameides et al. (1999) found that high aerosol loadings made crop losses in China from ground-based experiments. In contrast, the aerosol-induced radiation changes may pose a positive effect on vegetation growth. Due to the increasing ratio of diffuse radiation to total radiation caused by aerosols, diffuse radiation fertilization can increase the vegetation photosynthesis (Unger et al., 2017), especially in forest ecosystems, resulting in increased gross primary productivity (GPP) and net primary productivity (NPP). Zhang et al. (2020) found a significantly positive response of GPP to aerosols in forest ecosystems in China based on satellite observations. Xie et al. (2020) also found that aerosol held a positive impact on GPP in China through the coupled regional climate and interactive terrestrial biosphere models. However, with the continuously increase of aerosol loadings, it could also yield negative impacts on vegetation growth and photosynthesis (Yue et al., 2017b; Yue and Unger., 2018; Xue et al., 2020a). Last, aerosols can also change the temperature, evaporation rate and humidity, which leads to variations in photosynthesis and respiration in terrestrial ecosystems (Baldocchi, 2010; Jiang et al., 2019; Yue et al., 2017a; Zhang et al., 2019).

Previous studies mainly focused on exploring the comprehensive impacts on the terrestrial ecosystem of aerosols based on surface observations and couple models (Feng et al., 2019; Gao et al., 2018). However, most current models are fully coupled and failed to quantify the effects of ADRFs separately, leading to insufficient understanding of its impacts on terrestrial ecosystems. Therefore, the purpose of this study is to quantitatively calculate the ADRF and explore the aerosol direct radiation effect on terrestrial ecosystem carbon fluxes in China from a long-time series perspective. For this purpose, the Fu-Liou radiation transfer model combined with the land surface model is used to simulate carbon fluxes in China, including ecosystem productivity and respiration. In addition, a scenario without considering aerosols is evaluated to distinguish the quantitative effects of ADRF. The response of the environment variable to ADRF and its relationships with carbon fluxes are

then determined. Last, the variations in greenhouse gases productions across China are also investigated.

## 2. Study area, methodology and dataset

### 2.1. Study area

Significant spatial differences in climate features exist in mainland China, which could cause heterogeneities in the structure and physiological characteristics of vegetation. According to the National Assessment Report on Climate Change, seven subregions were delineated based on geographical and climatic characteristics (Ding et al., 2007), i.e., central, eastern, northern, southern, northeastern, northwestern and southwestern China. However, due to the unique vegetation types found at the high altitudes of the Qinghai-Tibet region, this area was extracted separately. The spatial distribution of the eight study areas is shown in Fig. 1.

### 2.2. Methodology

#### 2.2.1. Fu-Liou radiation transfer model

The Fu-Liou model has been exploited since the 1990s (Fu and Liou, 1991, 1993); then, it was modified to improve computing performance (Kato et al., 2005; Rose and Charlack, 2002). This model has a complete parameterization scheme of cloud optical properties. The impacts of clouds on radiation can be calculated through the input of cloud physical parameters by users. In addition, the radiation transfer mechanism can also be simulated in this model, making it more convenient than other models. This model has been widely used in related research on radiation, and a high estimation accuracy has been verified and evaluated (Huang et al., 2009; Xue et al., 2020a). In this paper, four radiation parameter networks across China, i.e., direct radiation, diffuse radiation, total radiation and diffuse fraction, were simulated and built by the Fu-Liou radiation transfer model. In addition, a scenario without aerosols (aerosol optical depth (AOD) = 0) was simulated to quantify the ADRF. The difference between those two scenarios was regarded as ADRF. In addition, the ratios between ADRF and the radiation fluxes under the no-aerosols scenario were also calculated, which was deemed the relative changes in radiation.

#### 2.2.2. Community Land Model

The Community Land Model 4.5 (CLM 4.5) is the third-generation land surface model developed by the National Center for Atmospheric Research (NCAR), which was released in June 2013 accompanied by the Community Earth System Model 1.2 (CESM 1.2). Compared with the previous version, the CLM 4.5 model contains a modified radiative transfer scheme and photosynthetic coefficient of the canopy to improve the simulation accuracy for GPP and other photosynthetic process parameters (Oleson et al., 2013). In addition, methane emissions from terrestrial ecosystems are considered in this model. Due to the excellent land surface process designs, ecosystem carbon fluxes could be captured in detail for each step. The CLM 4.5 model has been widely used in ecological and environmental science research, and the high simulation accuracy was verified by global surface-measured data collected over various underlying surfaces (Fu et al., 2016; Lawal et al., 2019). Four submodules, including biogeochemistry, biogeophysics, hydrological cycle and dynamic vegetation modules, exist in the CLM 4.5 model. In addition, this model can be coupled with the atmosphere, ocean and other modules to simulate the whole earth system. The operating mode of offline simulation was used in this paper, and the CLM4.5-BGC module, which covers the interaction between the terrestrial carbon cycle and nitrogen cycle, was selected to simulate the carbon fluxes in terrestrial ecosystems over China during 2001–2014. Before that, according to the user manuals, 1000 years of spin up and 200 years of final spin up were carried out to accelerate decomposition and obtain the initial field required for simulation for 2001. Then, accompanying the

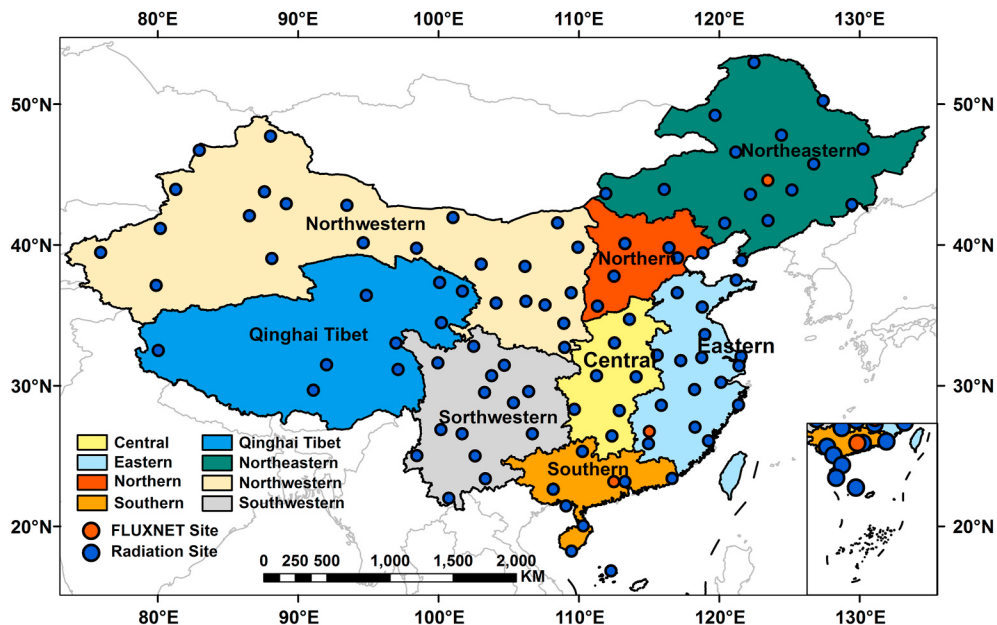


**Fig. 1.** Spatial distribution of the China Meteorological Administration (CMA) radiation and FLUXNET sites in China. The background map represents the eight study areas.

Fu-Liou estimated radiation datasets and other auxiliary datasets, the carbon fluxes were simulated based on this steady initial field over 14 years. Furthermore, we only changed the radiation (replacing the radiation dataset with the radiation under the no-aerosol scenario) to simulate the terrestrial carbon fluxes without aerosols. Similarly, the steady initial field for the no-aerosols scenario in 2001 was built, and the effects of ADRF on carbon fluxes are defined as the difference between those two scenarios. The carbon flux parameters used in this study include GPP, NPP, net ecosystem productivity (NEP), total ecosystem respiration (ER), autotrophic respiration (AR) and total heterotrophic respiration (HR), with a monthly temporal resolution and  $1.875^\circ \times 2.5^\circ$  spatial resolution. Additionally, the variation in the releases of  $\text{N}_2\text{O}$  and  $\text{CH}_4$  caused by ADRF was obtained to reflect the changes in other greenhouse gas emissions across China.

### 2.2.3. Analytical approach

Four statistical indicators were used in this study to evaluate the simulation results from the Fu-Liou and CLM 4.5 models. The linear correlation, overall estimation accuracy (whether overestimated or underestimated), absolute error and uncertainty compared with surface measurements are indicated by the Pearson correlation coefficient R, linear fitting, mean absolute error (MAE) and root mean square error (RMSE), respectively. To explore the temporal variations in the effects of ADRF on terrestrial ecosystem carbon fluxes in China, the monthly responses of carbon fluxes to aerosols were deseasonalized by calculating the monthly anomalies first. Then, those values were used to calculate the linear trends. The anomaly values were defined as the difference between the monthly mean value in one year and the monthly average values over the whole period. Then, we used the ordinary least squares fitting method to obtain the linear trend (Wei et al., 2021b). The paired-samples T-test was used to evaluate the statistical significance of those trends. Furthermore, to estimate the global warming effects caused by the changes in greenhouse gas production due to ADRF, this paper calculated the variations in GWP for  $\text{N}_2\text{O}$  and  $\text{CH}_4$  in the next 100 years according to the method of IPCC5 (Stocker et al., 2013) as follows:

$$GWP_{\text{N}_2\text{O}} = f\text{N}_2\text{O} \times \frac{44}{28} \times 265 \times S \quad (1)$$

$$GWP_{\text{CH}_4} = f\text{CH}_4 \times \frac{16}{12} \times 28 \times S \quad (2)$$

where  $GWP_{\text{N}_2\text{O}}$  and  $GWP_{\text{CH}_4}$  represent the changes in the global warming potential of  $\text{N}_2\text{O}$  and  $\text{CH}_4$ .  $f\text{N}_2\text{O}$  and  $f\text{CH}_4$  indicate the changes in the net production of  $\text{CH}_4$  and  $\text{N}_2\text{O}$  caused by the ADRF. Among them,  $\text{N}_2\text{O}$  flux is the sum of nitrifying  $\text{N}_2\text{O}$  and denitrifying  $\text{N}_2\text{O}$  fluxes, and the calculation of  $\text{CH}_4$  has excluded the amount of conversion from  $\text{CH}_4$  to  $\text{CO}_2$ .  $S$  indicates the area of different region.  $\frac{44}{28}$  and  $\frac{16}{12}$  represent the conversion factors to transform the masses of carbon and nitrogen into  $\text{CH}_4$  and  $\text{N}_2\text{O}$ , and the warming effects of 1 kg  $\text{CH}_4$  (unit: kg  $\text{CO}_2$  equivalent per kg  $\text{CH}_4$ ) and  $\text{N}_2\text{O}$  (unit: kg  $\text{CO}_2$  equivalent per kg  $\text{N}_2\text{O}$ ) in 100 years are 28 and 265 times than that of 1 kg  $\text{CO}_2$ , respectively.

### 2.3. Datasets

#### 2.3.1. Fu-Liou model input data

The MODIS collection 6.1 (C6.1) Level 3 combined dark target (DT) and deep blue (DB) algorithm AOD product with the highest quality assurance was selected as the input dataset of aerosols for the Fu-Liou model (Hsu et al., 2019). The temporal and spatial resolutions were 1 day and  $1^\circ \times 1^\circ$ , respectively. Before the model runs, the Terra and Aqua AODs were averaged to improve the spatial coverage of AOD first, and the mean AOD yielded excellent consistency compared with the surface measurement (Xue et al., 2020b). In addition, the cloud and meteorological parameters are also the requisite input datasets of the Fu-Liou model. The cloud parameters were collected from the CERES-SYN Edition 3a Level 3 cloud products with spatial and temporal resolutions of  $1^\circ \times 1^\circ$  and 3 h, respectively (Doelling et al., 2013), which includes seven characteristics, i.e., cloud-water content, effective radius of cloud water particles, cloud-ice content, effective scale of cloud ice particles, cloud top height, cloud bottom height and cloud fraction. Moreover, pressure, temperature and humidity profiles were collected from the National Centers for Environmental Prediction (NCEP)/National Centers for Atmospheric Research (NCAR). Additionally, we also calculated the AOD of seven aerosol types based on the proportion provided from the Modern-Era Retrospective Analysis for Research and Applications, version 2 (MERRA2) aerosol composition products (Gelaro et al., 2017), which cover black carbon, fine-mode dust, coarse-mode

dust, fine-mode sea salt, coarse-mode sea salt, organic carbon and sulfate. Single scattering albedo and asymmetry factor were obtained for different types of aerosols based on the setup of the optical properties in the Fu-Liou model, and they are listed in Table S1. All input datasets were resampled to the same spatial resolution as MODIS AOD based on the bilinear interpolation method.

### 2.3.2. CLM4.5 input data

Atmospheric forcing and land cover data are the essential input datasets for the CLM 4.5 model. The newest version (version 7) of the CRUNCEP atmospheric forcing datasets (Viovy, 2018), with temporal and spatial resolutions of 6 h and  $0.5^\circ \times 0.5^\circ$ , was selected in this paper to drive the land surface model which include radiation, precipitation, temperature, wind speed, humidity and pressure datasets. Based on this, the radiative forcing was modified with the results of the Fu-Liou model. To maintain a consistent spatial resolution, the Fu-Liou radiation datasets were interpolated to the same spatial resolution of  $0.5^\circ \times 0.5^\circ$  as the other atmospheric forcing datasets by the bilinear interpolation method. Compared with the original CRUNCEP radiative forcing data, the temporal resolution of the new input data was increased to 3 hour. However, the radiation of the CLM 4.5 model can be recognized as the total radiation only by default, and the diffuse radiation and direct radiation are calculated through the empirical formula based on total radiation. Therefore, two new variables (diffuse and direct radiation) were added manually in the CLM 4.5 model as valid input parameters based on the results of the Fu-Liou model, which increased the accuracy. Similarly, a radiation dataset without aerosols was built as the input radiative forcing data for the control scenario in this paper.

The land cover datasets used in the CLM 4.5 model were composed based on the methods of (Lawrence and Chase (2007)). In this dataset, the distributions of functional vegetation areas were synthesized by combining multiple satellite land cover products and matching the leaf area index. Initially, bare land and vegetation-covered areas were derived from moderate-resolution imaging spectroradiometer (MODIS) vegetation products (Hansen et al., 2003). Then, advanced very high resolution radiometer (AVHRR) continuous field tree cover was used to discriminate the tree types (Defries et al., 2000), which included broad-leaf, needle-leaf, evergreen and deciduous trees. Crop areas were distinguished on the basis of the global crop land area dataset (Ramankutty et al., 2008), and the grass and shrub regions were collected from the MODIS land cover products (Friedl et al., 2002). Furthermore, according to the physiology and climate rules put forward by Nemani and Running (1996), plants were divided into temperate, boreal and tropical functional types. Additionally, on the basis of the MODIS leaf area index (Still et al., 2003), the grass regions were divided into C3 and C4 regions. Overall, sixteen functional vegetation types were distinguished for the CLM 4.5 model.

### 2.3.3. Validation data

The monthly averaged radiation in situ measurement dataset from the CMA was selected as a comparison in this paper to verify the accuracy of the radiative forcing data. This dataset includes 99 sites for total radiation and 12 sites for diffuse radiation for the 2001–2014 period. The distribution of the radiation measurement sites is shown in Fig. 1, and numerous sites are distributed in each study area. The FLUXNET monthly averaged GPP and ER datasets (Pastorello et al., 2020) were used to evaluate the accuracy of the carbon fluxes simulation. However, the observation durations at each FLUXNET station in China were all short. To prevent errors caused by observation inconsistencies, three sites with the longest observation records and functional vegetation types similar to those in the CLM4.5 model were selected: QIA (26.74°N, 115.06°E), CNG (44.59°N, 123.51°E) and DIN (23.17°N, 112.54°E), which are located in eastern, northeastern and southern China, respectively (Fig. 1). The duration of the observation records for those three sites was 2003–2006, 2007–2011 and 2003–2006.

## 3. Results

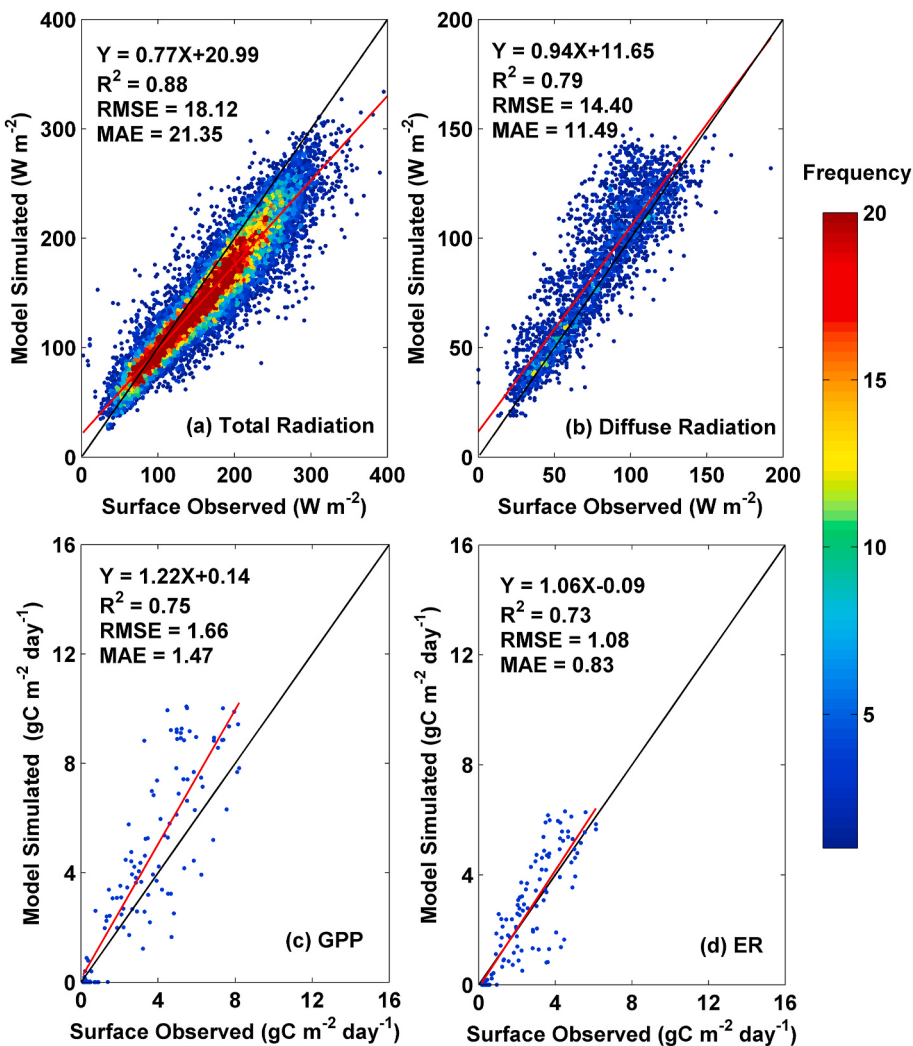
### 3.1. Model evaluation

Fig. 2 shows density scatterplots of the Fu-Liou model monthly radiation and CLM 4.5 carbon fluxes. The Fu-Liou model shows excellent estimated performance, with  $R^2$  (RMSE, MAE) values of 0.88 ( $18.12 \text{ W m}^{-2}$ ,  $21.35 \text{ W m}^{-2}$ ) and 0.79 ( $11.40 \text{ W m}^{-2}$ ,  $11.49 \text{ W m}^{-2}$ ) for total and diffuse radiation. In addition, good simulation abilities were maintained in forest, grass and farmland ecosystems, and these abilities were evaluated in our previous study (Xue et al., 2020a). The consistencies of GPP and ER have also been assessed in this paper. Because sixteen functional vegetation types were simulated in a pixel but only one type was confirmed at the corresponding ground observation site, the averaged rates of photosynthesis and respiration were uncertain. However, the correlations between the GPP simulated and measured data were satisfactory, with  $R^2$ , RMSE and MAE values of 0.75,  $1.66 \text{ gC m}^{-2} \text{ day}^{-1}$  and  $1.47 \text{ gC m}^{-2} \text{ day}^{-1}$ , respectively. Meanwhile, those indexes for ER were 0.73,  $1.08 \text{ gC m}^{-2} \text{ day}^{-1}$  and  $0.83 \text{ gC m}^{-2} \text{ day}^{-1}$ , respectively.

Figure S1 shows the temporal consistency between the simulation and measurement datasets for each site. Among all stations, the QIA station showed the highest consistency, with correlation coefficients  $R$  of 0.91 and 0.90 for GPP and ER, respectively. In contrast, the lowest  $R$  was found at the DIN station ( $R_{\text{GPP}} = 0.70$ ,  $R_{\text{ER}} = 0.87$ ) because of the lowest similarity of the functional vegetation types simulated in this pixel with those confirmed at the corresponding station. In addition, the errors associated with the radiation data could have also influenced the accuracy of the estimated carbon fluxes. Statistical indicators were calculated for each station, and the results indicated that the terrestrial ecosystem carbon fluxes were simulated well by the CLM 4.5 model (Table S2). Thus, this model can be used to explore the response of terrestrial ecosystem carbon fluxes to aerosols over China.

### 3.2. Aerosol-induced direct radiative forcing

Fig. 3 shows the seasonally averaged relative changes in radiation fluxes caused by aerosols in eight regions of China from 2001 to 2014, and the absolute aerosol radiative forcing is also exhibited in Figure S2. For all study areas, aerosols led to a significant increase in diffuse radiation and diffuse fraction and a conspicuous decrease in direct radiation and total radiation in all seasons. For diffuse radiation and fraction, the highest increases were determined in winter, with mean increases of 30.2% ( $\sim 11.21 \text{ W m}^{-2}$ ) and 51.2% ( $\sim 16.2\%$ ) compared to the no-aerosol scenario. The largest increases occurred in the northern region, which was up to 49.8% ( $14.46 \text{ W m}^{-2}$ ) and 73.3% (18.5%), respectively. Winter is the heating season in those areas, which mainly relies on fossil fuels during 2001–2004, causing abundant air pollutants (fine particles, NO<sub>x</sub> and SO<sub>2</sub>) to be generated and have positive impacts on diffuse radiation and factors. Furthermore, crop residue burning can also produce high levels of aerosol loading (Zhang et al., 2017). Remarkably, the positive effect was prominent in the northwestern area during autumn, which was caused by acute air pollution, and the change in diffuse radiation was approximately  $20.03 \text{ W m}^{-2}$ . For direct radiation, the greatest weakening was found in the central region for all seasons due to the high aerosol loading here, especially in spring, where the direct radiation decreased by 17.4% ( $\sim 21.43 \text{ W m}^{-2}$ ) because of aerosols. By comparison, the lowest negative impact existed in the Qinghai-Tibetan Plateau region, where it ranged from -8.4% ( $-29.94 \text{ W m}^{-2}$ ) to -6.2% ( $-23.63 \text{ W m}^{-2}$ ) over four seasons. In addition, the changes in total radiation show coincident spatial distribution with those of direct radiation. Considerable reductions in total radiation were captured in the central (-17.4% to -12.6%), eastern (-16.1% to -11.1%) and northern (-14.4% to -11.5%) regions, which possess high levels of urbanization and industrialization (Li et al., 2016). In general, the cut of total radiation in summer and autumn was significantly lower than that in winter and spring, and the highest average value was



**Fig. 2.** Density scatterplots of monthly averaged surface ground-observed and model-simulated radiation and carbon fluxes: (a)–(d) are total radiation, diffuse radiation, GPP and ER, respectively. The linear regression lines (red lines) and 1:1 lines (black lines) are also given. (For interpretation of the references to colour in this figure legend, the reader is referred to the Web version of this article.)

approximately  $-12.9\%$  in spring, as dust storm pollution occasionally covers most of China in this season and could have a serious negative impact on direct radiation, then total radiation would eventually decrease (Qian et al., 2002). In addition, since the total radiation fluxes in the Northern Hemisphere regions are higher in summer and spring than in other seasons, a higher reduction was also found in those seasons, especially in the northern region, which suffers from serious air pollution, with a change of  $-31.83 \text{ W m}^{-2}$  and  $-30.63 \text{ W m}^{-2}$ , respectively.

### 3.3. Response of carbon fluxes to aerosol radiative forcing

The terrestrial ecosystem carbon cycle, especially ecosystem photosynthesis and respiration, is quite sensitive to aerosol-induced direct radiation forcing (Rap et al., 2018). Table 1 lists the annual mean carbon flux differences caused by aerosol-induced direct radiation forcing across China. Compared with the no-aerosols scenario, the GPP increased by approximately  $3.20 \text{ gC m}^{-2}$  under the aerosol scenario in China as a whole. Meanwhile, AR and HR increased by  $5.08 \text{ gC m}^{-2}$  and  $0.05 \text{ gC m}^{-2}$ , respectively. In contrast, the NPP and NEP decreased significantly by  $1.88 \text{ gC m}^{-2}$  and  $1.93 \text{ gC m}^{-2}$ , respectively. However, sharp spatial heterogeneities in the responses of carbon fluxes to ADRF existed across China. ADRF could significantly weaken GPP in the central, eastern and Qinghai-Tibet regions, where its impacts were  $-26.44$

$\text{gC m}^{-2}$ ,  $-30.45 \text{ gC m}^{-2}$  and  $-16.73 \text{ gC m}^{-2}$ , respectively, while aerosols increased GPP by  $12.12 \text{ gC m}^{-2}$  to  $28.38 \text{ gC m}^{-2}$  in other regions. Similar distributions were found in ER, and the highest and lowest change was captured in the northern ( $26.44 \text{ gC m}^{-2}$ ) and eastern ( $-27.94 \text{ gC m}^{-2}$ ) regions. The spatial variability is mainly caused by the differences in vegetation types and aerosol loadings. Especially for the Qinghai-Tibet region, the major vegetation function type introduced in CLM4.5 is C3 Arctic grass, which is quite fragile (Jiang et al., 2020). The photosynthesis of vegetation will be affected by the variations in environmental conditions caused by a decrease in direct radiation, especially in the growing season of vegetation (summer). In contrast, forest and farmland ecosystems dominate in the central and eastern regions. Although the canopy structures of vegetation are conducive to the absorption and utilization of diffuse radiation increased by aerosols, the direct radiation loss caused by aerosols has more negative impacts on the photosynthesis of vegetation in the two regions. The drop in direct radiation will lead to a decrease in photosynthetically active radiation and light passing through the canopy, which could cause a reduction in the photosynthetic rates of sunlit leaves and shaded leaves. At the same time, the varieties of external hydrothermal conditions in different regions will also cause changes in GPP. Notably, due to the diffusing fertilization effect, positive impacts of aerosols on NPP were captured in the northern, northeastern, northwestern and southwestern regions, ranging from  $0.29 \text{ gC m}^{-2}$  to  $14.84 \text{ gC m}^{-2}$ . The leaf area index of

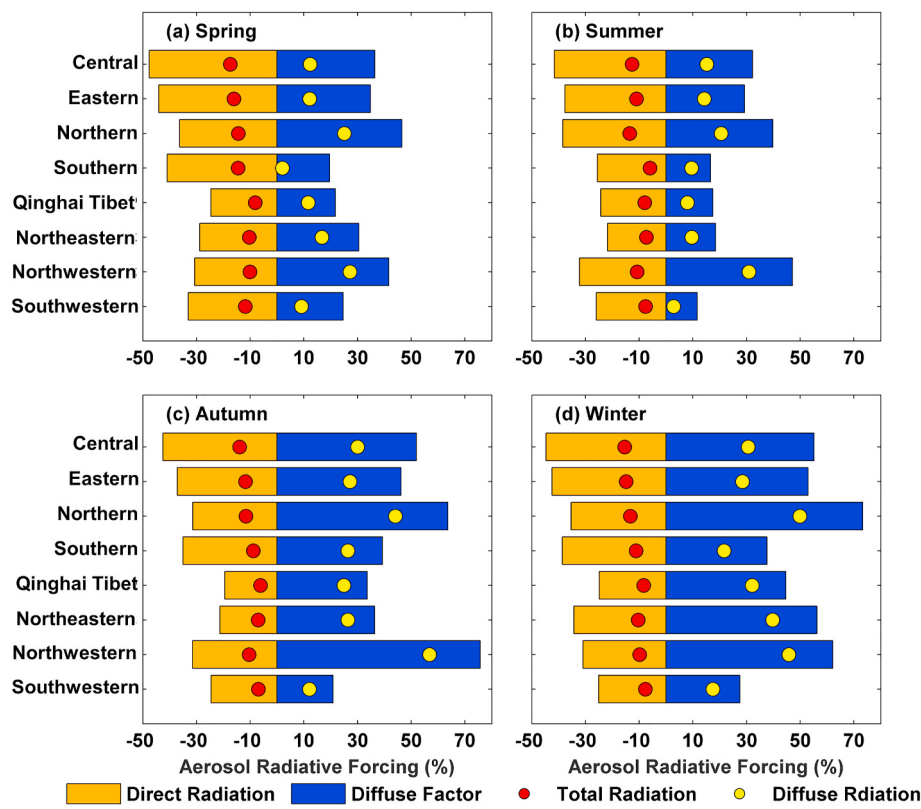


**Fig. 3.** The seasonally averaged relative changes in radiation fluxes caused by aerosols from 2001 to 2014 over China. (a)–(d) was Spring (Mar-Apr-May), summer (Jun-Jul-Aug), autumn (Sep-Oct-Nov) and winter (Dec-Jan-Feb), respectively.

**Table 1**  
Annual averaged differences in carbon fluxes caused by ADRF in China.

Region	GPP (gC m <sup>-2</sup> )	NPP (gC m <sup>-2</sup> )	NEP (gC m <sup>-2</sup> )	ER (gC m <sup>-2</sup> )	AR (gC m <sup>-2</sup> )	HR (gC m <sup>-2</sup> )
Central	-26.44	-18.88	-6.33	-20.11	-7.56	-12.55
Eastern	-30.45	-24.44	-2.51	-27.94	-6.01	-21.93
Northern	28.35	14.84	1.91	26.44	13.51	12.93
Southern	13.56	-20.63	-0.12	13.68	34.19	-20.51
Qinghai Tibet	-16.73	-9.43	-3.53	-13.2	-7.30	-5.90
Northeastern	17.03	8.73	-3.72	20.75	8.30	12.45
Northwestern	16.07	8.99	2.42	13.65	7.08	6.57
Southwestern	12.12	0.29	-4.59	16.71	11.83	4.88
China	3.20	-1.88	-1.93	5.13	5.08	0.05

shaded leaves was much higher than that of sunlit leaves, which could absorb and utilize more diffuse radiation. Thus the positive influences were higher than the negative influence of ADRF on leaf photosynthesis in these regions. In addition, coincident variations in NEP and NPP were found in all areas, except for the northeastern and southwestern regions. The main reason for the inconformity between the two carbon fluxes was HR. Abundant microorganisms and nutrients existed in the soil, which could result in the high sensitivity of HR to variations in hydrothermal conditions caused by aerosols.

Due to obvious seasonal variations in radiation fluxes, the impacts of ADRF on carbon fluxes also possess general seasonal pattern. Table S3 lists the seasonally averaged differences in carbon fluxes caused by ADRF across China. Significant increases in GPP occur in autumn and summer. Especially in summer, the positive impact was  $8.16 \text{ gC m}^{-2} \text{ season}^{-1}$ , while the increases in NPP and ER were  $3.85 \text{ gC m}^{-2} \text{ season}^{-1}$  and  $4.12 \text{ gC m}^{-2} \text{ season}^{-1}$ , respectively. During this season, the enhancements of diffuse fraction are conducive to photosynthesis and referred to as diffusing fertilization effects. In addition, the decrease in

direct radiation was relatively low, and these two effects collectively result in the accumulation of carbon in terrestrial ecosystems. In contrast, in winter and spring, ADRF had negative effects on GPP, which caused GPP to drop by  $2.05 \text{ gC m}^{-2} \text{ season}^{-1}$  and  $5.21 \text{ gC m}^{-2} \text{ season}^{-1}$ , respectively. In addition, inconsistencies in the responses of photosynthesis and respiration to ADRF existed in China. Especially in spring, the impacts of ADRF on ER and HR were positive, while they were negative on NPP and NEP, with decreases of  $3.32 \text{ gC m}^{-2} \text{ season}^{-1}$  and  $5.33 \text{ gC m}^{-2} \text{ season}^{-1}$ , respectively. This indicates that the indirect effects of changes in environmental variables caused by ADRFs on terrestrial ecosystems in China may be stronger than the diffusing fertilization effects caused by ADRFs.

Fig. 4 shows the spatial distributions of relative differences of carbon fluxes caused by ADRF across China for four seasons. In most areas, ADRF can promote vegetation photosynthesis in summer and autumn. Especially in summer, the highest increases appear in the northwestern region; compared with the no ADRF scenarios, GPP increases by approximately 12.2%. In contrast, ADRF will limit vegetation photosynthesis in winter across large areas of China, except for the southern and southwestern regions. During this season, most areas of China were exposed to high aerosol loading, as a result the direct radiation used for photosynthesis was largely lost. Furthermore, vegetation has completed the defoliation process in winter, and a low leaf area index is not conducive to the absorption of diffuse radiation, which will eventually lead to a decrease in GPP, NPP and NEP. Notably, significant losses of GPP were determined in the Qinghai-Tibet region for the four seasons, with a range from  $-8.0\%$  to  $-2.2\%$ . C3 Arctic grass is the main vegetation function type in this area. This vegetation function type possesses the characteristics of a small leaf area index, simple vegetation structures and low photosynthetic intensity, resulting in high sensitivity to radiation changes. As mentioned in section 3.2, aerosols caused a significant drop in total radiation in this region; thus, photosynthesis may be limited. The results indicated that the decrease range of NPP (NEP) in

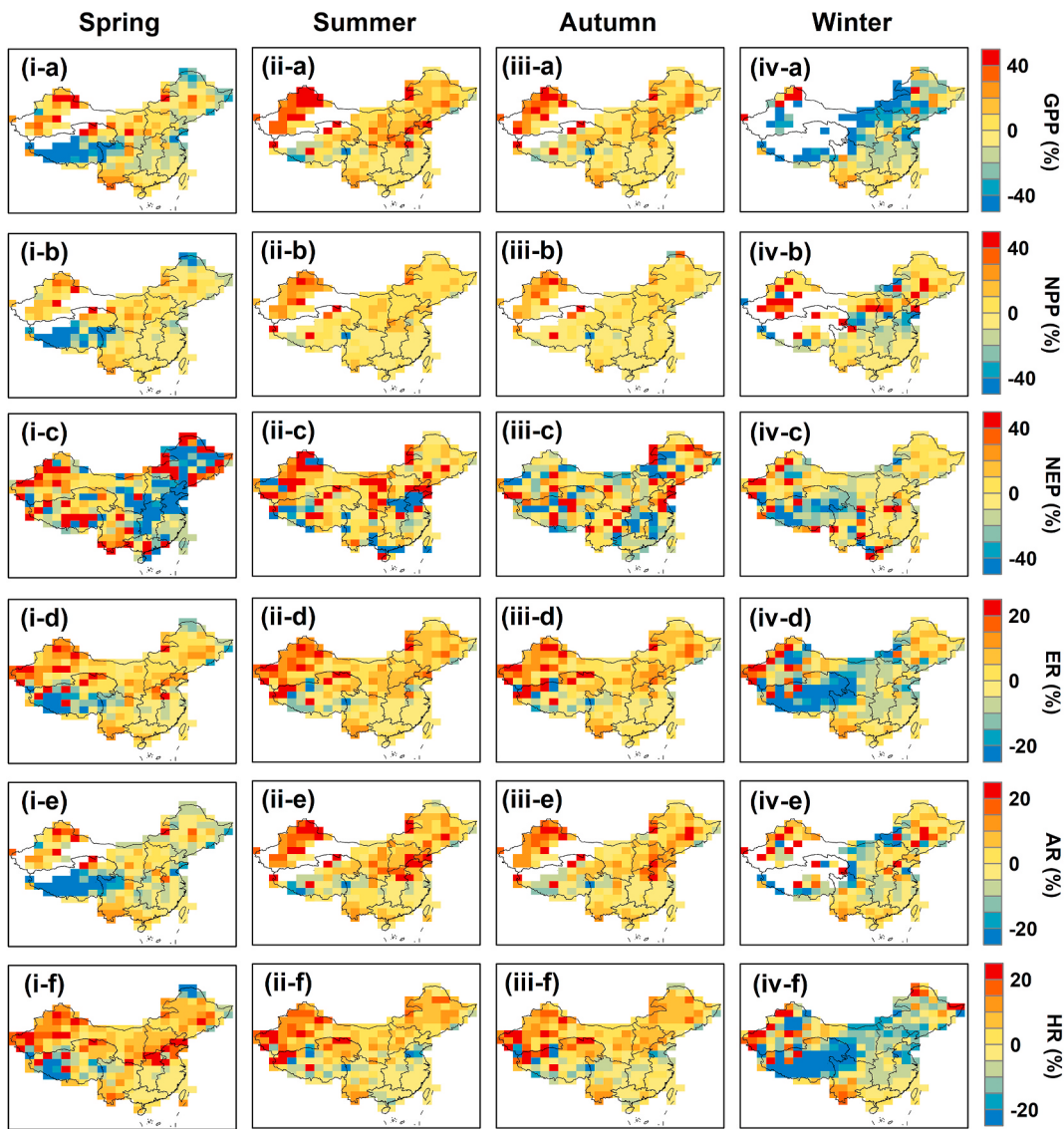


**Fig. 4.** The spatial distributions of relative carbon flux differences caused by ADRF across China from 2001 to 2014. (i) – (iv) for spring, summer, autumn and winter; (a)–(f) for GPP, NPP, NEP, ER, AR and HR, respectively.

the Qinghai-Tibet region was from  $-4.9\%$  to  $-2.4\%$  ( $-9.5\%$  to  $-1.6\%$ ). For respiratory fluxes, almost all regions had negative responses to ADRFs in winter, and more intense effects were found on HR than on AR. Especially in the northern region, the effect was approximately  $-5.1\%$ . According to the principle of energy conservation, due to the reduction in total radiation, energy reaching the ground is also reduced. It will lower the surface temperature, thus limiting ecosystem respiratory intensity.

From 2001 to 2014, aerosol loading exhibited a trend of increasing early and then decreasing later across China (Xue et al., 2020a). Meanwhile, ADRF also varied during this period, which could cause temporal variations in the effects on carbon fluxes. Fig. 5 shows the temporal trends of carbon flux changes caused by ADRF across China from 2001 to 2014. The temporal trends for the three phases were calculated in this study, including 2001–2007, 2008–2014 and 2001–2014. Overall, the variation in the effect on GPP was insignificant, with a trend of  $-0.10 \text{ gC m}^{-2} \text{ year}^{-1}$  ( $p > 0.1$ ). A statistically significant temporal trend was observed in 2001–2007 due to the enhancement of diffusing fertilization effects, with an increasing trend of  $3.47 \text{ gC m}^{-2} \text{ year}^{-1}$  ( $p < 0.01$ ). In contrast, a decreasing trend of the changes in GPP was captured after 2007, with a trend of  $-1.51 \text{ gC m}^{-2} \text{ year}^{-1}$  ( $p > 0.1$ ),

which indicated that the reduction in ecosystem production caused by the decrease in direct radiation exceeded the enhancement caused by the diffusing fertilization effect. However, due to the interference of respiratory fluxes, the temporal trends of NPP and NEP did not reach the statistical significance level for those three phases. For respiration fluxes, the temporal trend for the changes in ER caused by ADRF significantly increased from 2001 to 2007 by  $2.93 \text{ gC m}^{-2} \text{ year}^{-1}$  ( $p < 0.01$ ), while it was  $2.19 \text{ gC m}^{-2} \text{ year}^{-1}$  ( $p < 0.01$ ) from 2008 to 2014. Compared with HR, AR contributed more to this variation, with trends for 2001–2007 and 2008–2014 of  $3.10 \text{ gC m}^{-2} \text{ year}^{-1}$  ( $p < 0.01$ ) and  $-1.49 \text{ gC m}^{-2} \text{ year}^{-1}$  ( $p < 0.01$ ), respectively.

#### 3.4. Changes of soil water and heat conditions

Because we selected the offline method for the CLM4.5 simulation, the atmospheric parameters are forced every 6 hours; therefore, the simulation process will cover up its impact on air environmental variables. Although environmental variables, e.g., 2-m humidity and wind speed, will change due to the variation in radiation fluxes, significant differences exist compared with the coupled model, which can only be performed for qualitative analysis. Therefore, we only conduct

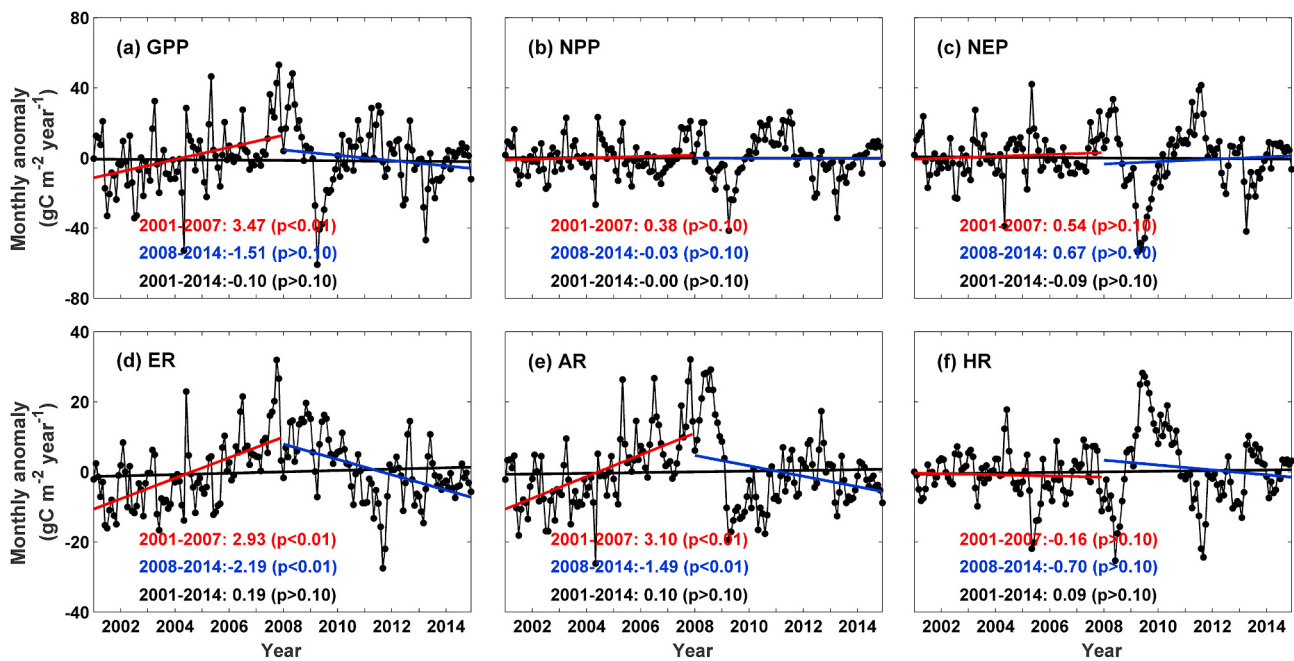


**Fig. 5.** The temporal trends of deseasonalized monthly responses of carbon flux to aerosol radiative forcing anomalies over China from 2001 to 2014. (a)–(f) GPP, NPP, NEP, ER, AR and HR, respectively. The red, blue and black lines denote the trends from 2001 to 2007, 2008–2014 and 2001–2014, respectively. (For interpretation of the references to colour in this figure legend, the reader is referred to the Web version of this article.)

quantitative analysis for the environmental parameters involved in the land surface processes, which includes soil temperature in the top 0.1 m of soil (unit: K) and volumetric soil water (unit:  $\text{mm}^3 \text{mm}^{-3}$ ). In the CLM4.5 model, the soil layer was divided into 15 layers (from 0 to 40.10 m). Here, we only calculated the total soil water content of the top five layers, and the specific structures are listed in Table 2.

Fig. 6 shows the changes in soil water and heat conditions caused by ADRFs in China. Due to the cooling effects of aerosols (Krishnan and Ramanathan, 2002), negative impacts on soil temperature were observed, and significant numerical spatial heterogeneities existed across China. Overall, the northern region exhibits the most intense temperature response, with average reductions in the soil temperature of approximately  $0.92 \pm 0.18$  K. In contrast, due to the low aerosol loading, the changes in southern regions were lowest, with a decrease of  $0.31 \pm 0.13$  K. Notably, the Qinghai-Tibet region expressed a large drop in soil temperature, which was approximately  $0.66 \pm 0.11$  K. In this area, temperature is one of the main limiting factors for vegetation growth, and a decrease in soil temperature will inevitably lead to a weakening of photosynthesis. However, from another perspective, the cooling effect caused by aerosols will curb global warming processes. Meanwhile, following the rules of the Clausius Clapeyron equation, due to the decreases in radiation and temperature, the saturated vapor pressure of water vapor will decrease, which leads to a reduction in evaporation, eventually resulting in an increase in volumetric soil water. Due to the high moisture content of the soil in the central and eastern regions, the disturbances of ADRF for volumetric soil water are greater here, which express relatively high increases of  $0.057 \pm 0.013 \text{ mm}^3 \text{mm}^{-3}$  and  $0.050 \pm 0.013 \text{ mm}^3 \text{mm}^{-3}$ , respectively. In contrast, a slight change existed in the northwestern region, with an increase of approximately  $0.017 \pm 0.004 \text{ mm}^3 \text{mm}^{-3}$ . In addition, although the soil moisture content in the southern area was higher, because of the low

aerosol loading, the impact on volumetric soil water by ADRF was also low, which was  $0.024 \pm 0.006 \text{ mm}^3 \text{mm}^{-3}$ .

The changes in the soil water and heat conditions can also affect carbon fluxes. To explore their relationship, we calculated the temporal correlation coefficients ( $r$ ) among them from 2001 to 2014. Fig. 7 expresses the relationship for the changes in soil temperature, volumetric soil water and carbon fluxes induced by ADRF in the eight regions. Due to the significant differences in environmental sensitivity of ecosystems across each region, three relationships existed in China: strong correlation (northeastern region), moderate correlation (eastern, southern, northwestern and southwestern region) and weak correlation (central, northern and Qinghai Tibet region). In the northeastern region, photosynthesis and respiration were considerably impacted by soil water and heat conditions. Compared with volumetric soil water, the changes in soil temperature are more correlated with photosynthetic fluxes. In terms of time series, significant negative correlations were captured for GPP and NPP, with  $r$  values of  $-0.60$  ( $p < 0.05$ ) and  $-0.60$  ( $p < 0.05$ ), respectively. In contrast, respiratory flux was more sensitive to volumetric soil water, with significant positive correlations of  $0.64$  ( $p < 0.05$ ) between AR and volumetric soil water. This area is located at high latitudes, and temperature and radiation play a critical role in vegetation growth. In addition, those effects could also alter the exchange of  $\text{CO}_2$  here. For the moderate-correlation regions, the influences of temperature were dominant in all regions, and only a significant positive correlation was captured in the northwestern region between AR and volumetric soil water, with an  $r$  of  $0.52$  ( $p < 0.1$ ). Arid and semiarid areas in China are mostly distributed in this region, and water is one of the main limiting factors for vegetation growth; therefore, the enhancement of soil water promoted the carbon flux increase here. In other moderate-correlation regions, the highest temporal correlation coefficients were all captured between soil temperature and ER, which were  $-0.65$  ( $p < 0.05$ ),  $-0.80$  ( $p < 0.01$ ) and  $-0.59$  ( $p < 0.05$ ) in the eastern, southern and southwestern regions, respectively. For weakly correlated regions, none of the responses of photosynthesis and respiration to soil water and heat conditions were statistically significant in the Qinghai-Tibet region, which indicated that the changes in soil water and heat conditions were not crucial factors for carbon flux changes. In

**Table 2**  
The structure of soil layers in CLM4.5 model. (unit: meter).

	Layer1	Layer2	Layer3	Layer4	Layer5
Depth at layer interface	0.0175	0.0276	0.0455	0.0750	0.1236
Soil column	0.0175	0.0451	0.0906	0.1655	0.2891

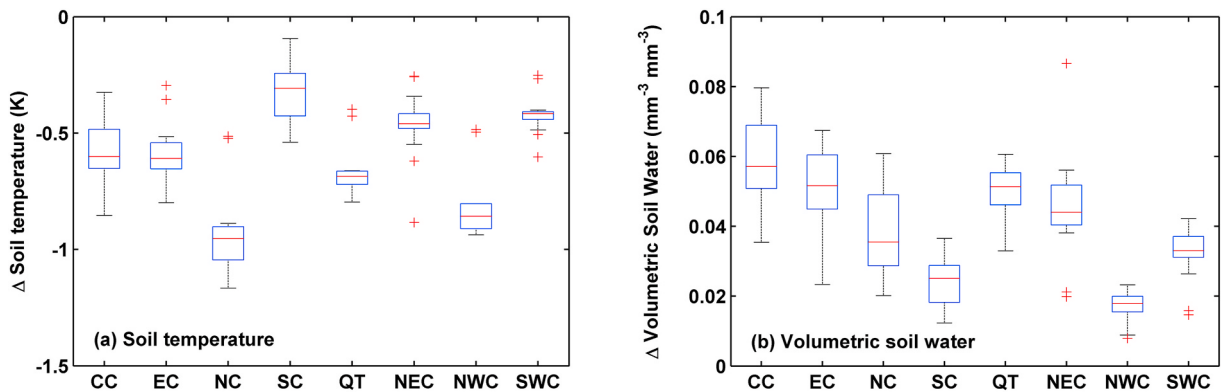


**Fig. 6.** The responses of soil water and heat conditions to ADRF among the eight study areas from 2001 to 2014. (a)–(b) are soil temperature and volumetric soil water; CC, EC, NC, SC, QT, NEC, NEC and SWC represent the central, eastern, northern, southern, Qinghai Tibet, northeastern, northwestern and southwestern regions, respectively.

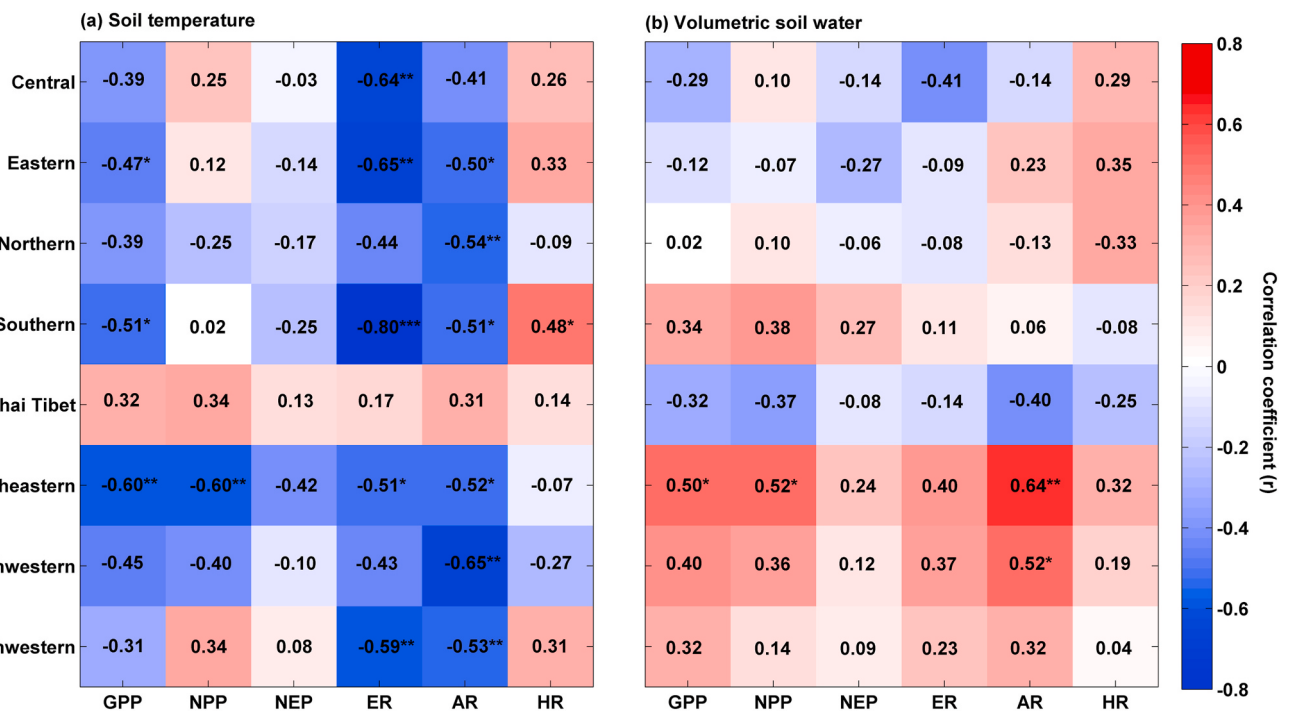


**Fig. 7.** The relationships between the changes in soil water and heat conditions and carbon fluxes induced by ADRFs across China. (a)–(b) Soil temperature and volumetric soil water; \*, \*\* and \*\*\* indicate confidence at the 90%, 95% and 99% levels, respectively.

this region, C3 arctic grass is the major vegetation functional type as described in CLM4.5, which is fragile and sensitive. Therefore, the direct effects of ADRF are more obvious here than the indirect effects (changes in soil water and heat conditions) on terrestrial ecosystem carbon fluxes.

#### 4. Discussions

Due to the changes in soil water and heat conditions,  $\text{N}_2\text{O}$  and  $\text{CH}_4$  production in soil will also be altered. Figure S3 shows the changes in  $\text{N}_2\text{O}$  and  $\text{CH}_4$  production caused by ADRF in eight areas across China. ADRF can increase  $\text{CH}_4$  production in all regions, especially in the northeastern region, with an annual mean enhancement of approximately 0.045 TgC. For the changes in  $\text{N}_2\text{O}$ , in general, ADRF will cause it to increase significantly in most areas across China, which covered the range of 0.000–0.015 TgN year<sup>-1</sup>. However, it decreased in the southwestern and central regions. Then, based on the method of IPCC 5

introduced in section 2, we calculated the variations in GWPs for greenhouse gases in the next 100 years. Fig. 8 shows the changes of  $\text{CH}_4$  and  $\text{N}_2\text{O}$  GWPs caused by ADRFs in China. In general, ADRFs will enhance both the  $\text{CH}_4$  and  $\text{N}_2\text{O}$  GWP across China. Although the change in  $\text{CH}_4$  release was greater than that of  $\text{N}_2\text{O}$ , due to the greater warming effects, the GWP of  $\text{N}_2\text{O}$  was higher, with changes in the GWP of 17.82 Tg CO<sub>2</sub> equivalent year<sup>-1</sup> and 3.01 Tg CO<sub>2</sub> equivalent year<sup>-1</sup>, respectively. The  $\text{CH}_4$  GWP, due to the ADRF, has increased in all regions of China. The highest increase was captured in the northeastern region, which increased by approximately 1.69 Tg CO<sub>2</sub> equivalent year<sup>-1</sup>, accounting for 56.1% of the whole GWP in China. The contents of soil organic matter and microorganisms are high in this area, and the increase in soil water content caused by ADRF leads to the enhancement of anaerobic respiration and methane production. In addition, this area is one of the main rice growing areas in China, where large amounts of methane will be released. In addition, the changes of the  $\text{CH}_4$  GWP in the Qinghai-Tibet region is also high, accounting for approximately 14.6%

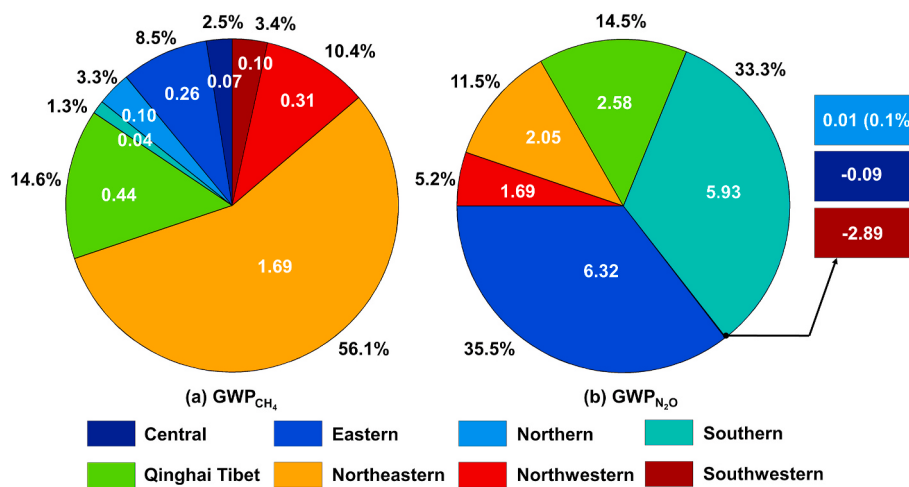


**Fig. 8.** The GWP changes in  $\text{CH}_4$  and  $\text{N}_2\text{O}$  production caused by ADRF in China.

of all. In contrast, the changes in  $\text{CH}_4$  GWP in the southern region were smaller, with a proportion of only 1.3%. However, the change in  $\text{N}_2\text{O}$  GWP was high in this region, at 5.93 Tg  $\text{CO}_2$  equivalent year<sup>-1</sup>. Similar high changes existed in eastern areas, and the positive effects on  $\text{N}_2\text{O}$  GWP caused by ADRF were 6.32 Tg  $\text{CO}_2$  equivalent year<sup>-1</sup>. In contrast, negative effects were found in the central and southwestern regions, with changes of -0.09 Tg  $\text{CO}_2$  equivalent year<sup>-1</sup> and -2.89 Tg  $\text{CO}_2$  equivalent year<sup>-1</sup>. From the aspect of results, the influences of ADRF on  $\text{CH}_4$  and  $\text{N}_2\text{O}$  GWP mainly depend on two aspects, i.e., aerosol loading and vegetation functional types.

In our work, the Community Atmosphere Model (CAM) has not been coupled, and aerosol-induced indirect radiation effects, e.g., variations in precipitation, ambient temperature and humidity, are not considered in this study. However, almost all previous coupling results show that aerosols can cause cooling effects (Jim, 2005; Unger et al., 2017; Zhang et al., 2019). This indicates that the global warming effect of  $\text{CH}_4$  and  $\text{N}_2\text{O}$  production caused by the direct radiation effect of aerosols will eventually be offset by the indirect radiation effect of aerosols.

## 5. Conclusions

In this work, the influences of aerosol-induced direct radiation forcing on carbon fluxes from 2001 to 2014 across China were investigated. First, we used the Fu-Liou radiation transfer model to simulate the radiation fluxes across China from 2001 to 2014, and the results show that the Fu-Liou model is accurate in estimating radiation fluxes ( $R^2 = 0.79\text{--}0.88$ ) across China. In addition, radiation fluxes under the no-aerosol scenario are estimated according to this model. Through the comparison of radiation fluxes under two scenarios, the ADRF was estimated. The results indicated that aerosols can significantly reduce direct radiation and enhance diffuse radiation, especially during winter. Furthermore, due to the differences in aerosol loading, significant spatial heterogeneity of ADRF was captured in China. Afterward, to evaluate the impacts of ADRF on carbon fluxes of terrestrial ecosystems, we used the results of the Fu-Liou model under aerosol and no-aerosol scenarios to modify the atmospheric forcing datasets. Then, combined with the CLM4.5 model, the carbon fluxes under those two scenarios are also estimated. The simulated carbon fluxes under the aerosol scenario also show high consistency with the ground observations ( $R^2 = 0.73\text{--}0.75$ ). Comparative analyses show that ADRF can cause diffusing fertilization effects in most areas of China, resulting in 3.20  $\text{gC m}^{-2}$  and 5.13  $\text{gC m}^{-2}$  increases in GPP and ER in terrestrial ecosystems per year, respectively, especially in the northern region. In contrast, due to high aerosol loading in central China, the loss of GPP caused by a decrease in direct radiation is greater than that of diffusing fertilization effects.

However, changes in aerosol types and loadings also lead to significant seasonal heterogeneity, and temporal variations in diffusing fertilization effects exist in China. Almost all carbon flux changes caused by ADRFs first increased and then decreased in China from 2001 to 2014. Furthermore, to explain the potential impact mechanism between ADRF and carbon fluxes, the soil temperature and volumetric soil water are also simulated under those two scenarios. ADRF can reduce soil temperature and enhance volumetric soil water, which are closely related to changes in carbon fluxes. Among most regions, the responses of respiration and photosynthesis fluxes to ADRF are more sensitive to soil temperature. Finally, due to the changes in soil water and heat conditions, the production of  $\text{CH}_4$  and  $\text{N}_2\text{O}$  in the soil generally increases, resulting in an increase in  $\text{CH}_4$  and  $\text{N}_2\text{O}$  global warming potential. Therefore, the reasonable control of atmospheric aerosol pollution in China has important implications for alleviating global warming and peaking carbon dioxide emissions before 2030 and achieving carbon neutrality before 2060.

## Declaration of competing interest

The authors declare that they have no known competing financial interests or personal relationships that could have appeared to influence the work reported in this paper.

## Acknowledgments

This study was supported by the National Natural Science Foundation of China (41575144) and the National Key R&D Program of China (2017YFA0603603). We gratefully acknowledge Prof. Liou and Prof. Fu for provision of the source code of the Fu-Liou radiation transfer model. The radiation situ-observed data used in this study are available from the China Meteorological Administration (<http://data.cma.cn/>). The carbon flux in situ-observed data used in this study are available from FLUXNET (<https://fluxnet.org/>). The atmospheric forcing data for the Community Land Model are available from the NCAR/UCAR (<https://rd.a.ucar.edu/datasets/ds314.3/>).

## Appendix A. Supplementary data

Supplementary data to this article can be found online at <https://doi.org/10.1016/j.envres.2021.111464>.

## References

- Baldocchi, D.D., 2010. Measuring and modelling carbon dioxide and water vapour exchange over a temperate broad-leaved forest during the 1995 summer drought. *Plant Cell Environ.* 20 (9), 1108–1122.
- Bartell, S.M., Longhurst, J., Tjoa, T., et al., 2013. Particulate air pollution, ambulatory heart rate variability, and cardiac arrhythmia in retirement community residents with coronary artery disease. *Environ. Health Perspect.* 121, 1135–1141.
- Bellouin, N., Rae, J., Jones, A., et al., 2011. Aerosol forcing in the climate model intercomparison project (CMIP5) simulations by HadGEM2-ES and the role of ammonium nitrate. *J. Geophys. Res.* 116, D20206.
- Chameides, W.L., Yu, H., Liu, S.C., et al., 1999. Case study of the effects of atmospheric aerosols and regional haze on agriculture: an opportunity to enhance crop yields in China through emission controls? *Proc. Natl. Acad. Sci. U. S. A.* 96 (24), 13626–13633.
- Chan, C.K., Yao, X., 2008. Air pollution in mega cities in China. *Atmos. Environ.* 42 (1), 1–42.
- Charlson, R.J., Schwartz, S.E., Hales, J.M., et al., 1992. Climate forcing by anthropogenic aerosols. *Science* 255 (5043), 423–430.
- Che, H., Qi, B., Zhao, H., Xia, X., Eck, T.F., Goloub, P., Dubovik, O., Estelles, V., Cuevas-Agulló, E., Blarel, L., Wu, Y., Zhu, J., Du, R., Wang, Y., Wang, H., Gui, K., Yu, J., Zheng, Y., Sun, T., Chen, Q., Shi, G., Zhang, X., 2018. Aerosol optical properties and direct radiative forcing based on measurements from the China Aerosol Remote Sensing Network (CARSNET) in eastern China. *Atmos. Chem. Phys.* 405–425. <https://doi.org/10.5194/acp-18-405-2018>.
- Chen, J.L., He, L., Yang, H., Ma, M., Chen, Q., Wu, S.J., et al., 2019. Empirical models for estimating monthly global solar radiation: a most comprehensive review and comparative case study in China. *Renew. Sustain. Energy Rev.* 108, 91–111.
- DeFries, R.S., Hansen, M.C., Townshend, J.R.G., et al., 2010. A new global 1km dataset of percentage tree cover derived from remote sensing. *Global Change Biol.* 6 (2), 247–254.
- Ding, Y., Ren, G., Shi, G., 2007. China's national assessment report on climate change (summary). *World Environ.* 3, 1–5.
- Doelling, D.R., Loeb, N.G., Keyes, D.F., et al., 2013. Geostationary enhanced temporal interpolation for CERES flux products. *J. Atmos. Ocean. Technol.* 30, 1072–1090.
- Fan, J., Wu, L., Zhang, F., et al., 2019. Empirical and machine learning models for predicting daily global solar radiation from sunshine duration: a review and case study in China. *Renew. Sustain. Energy Rev.* 100, 186–212.
- Feng, Y., Chen, D., Zhao, X., 2019. Impact of aerosols on terrestrial gross primary productivity in north China using an improved boreal ecosystem productivity simulator with satellite-based aerosol optical depth. *GIScience Remote Sens.* 57 (5), 1–13.
- Plato, G., Marotzke, J., Abiodun, B., et al., 2013. Evaluation of climate models. In: *Climate Change 2013: the Physical Science Basis. Contribution of Working Group I to the Fifth Assessment Report of the Intergovernmental Panel on Climate Change, Computational Geometry*, vol. 18, pp. 95–123, 2.
- Friedl, M.A., McIver, D.K., Hodges, J.C.F., et al., 2002. Global land cover mapping from MODIS: algorithms and early results. *Remote Sens. Environ.* 83 (1–2), 287–302.
- Fu, C., Wang, G., Goulden, M.L., Scott, R.L., Bible, K., G Cardon, Z., 2016. Combined measurement and modeling of the hydrological impact of hydraulic redistribution using clm4.5 at eight Ameriflux sites. *Hydroclim. Earth Syst. Sci.* 20 (5), 1–33.
- Fu, Q., Liou, K.N., 1993. Parameterization of the radiative properties of cirrus clouds. *J. Atmos. Sci.* 50 (13), 2008–2025.
- Fu, Qiang, Liou, K.N., 1991. On the correlated k-distribution method for radiative transfer in nonhomogeneous atmospheres. *J. Atmos. Sci.* 49 (22), 2139–2156.
- Gao, X., Gu, F., Mei, X., et al., 2018. Light and water use efficiency as influenced by clouds and/or aerosols in a rainfed spring maize cropland on the loess plateau. *Crop Sci.* 58 (2), 853–862.
- Gelaro, R., McCarty, W., Suarez, M.J., et al., 2017. The modern-era retrospective analysis for research and applications, version 2 (MERRA-2). *J. Clim.* 30, 5419–5454.
- Greenwald, R., Bergin, M.H., Xu, J., et al., 2006. The influence of aerosols on crop production: a study using the CERES crop model. *Agric. Syst.* 89 (2), 390–413.
- Gu, L.H., Baldocchi, D.D., Wofsy, S.C., et al., 2003. Response of a deciduous forest to the Mount Pinatubo eruption: enhanced photosynthesis. *Science* 299 (5615), 2035–2038.
- Hansen, M., DeFries, R.S., Townshend, J.R.G., et al., 2003. Global percent tree cover at a spatial resolution of 500 meters: first results of the MODIS vegetation continuous fields algorithm. *Earth Interact.* 7 (10), 1–15.
- Haywood, J., Boucher, O., 2000. Estimates of the direct and indirect radiative forcing due to tropospheric aerosols: a review. *Rev. Geophys.* 38 (4), 513–543.
- Hsu, N.C., Lee, J., Sayer, A.M., et al., 2019. VIIRS deep blue aerosol products over land: extending the EOS long-term aerosol data records. *J. Geophys. Res.* 124, 4026–4053.
- Huang, J., Fu, Q., Su, J., Tang, Q., Minnis, P., Hu, Y., Yi, Y., Zhao, Q., 2009. Taklimakan dust aerosol radiative heating derived from CALIPSO observations using the Fu-Liou radiation model with CERES constraints. *Atmos. Chem. Phys.* 4011–4021.
- Huang, J., Wang, T., Wang, W., et al., 2015. Climate effects of dust aerosols over east Asian arid and semiarid regions. *Journal of Geophysical Research-atmospheres* 119 (19), 11398–11416.
- Huang, M., Crawford, J.H., Carmichael, G.R., et al., 2020. Impact of aerosols from urban and shipping emission sources on terrestrial carbon uptake and evapotranspiration: a case study in east Asia. *J. Geophys. Res.: Atmosphere* 125 (2), 1–23.
- Huang, X., Ding, A., Liu, L., et al., 2016. Effects of aerosol-radiation interaction on precipitation during biomass-burning season in East China. *Atmos. Chem. Phys.* 16, 10063–10082.
- Jia, R., Liu, Y., Hua, S., et al., 2018. Estimation of the aerosol radiative effect over the Tibetan plateau based on the latest calipso product. *Journal of Meteorological Research* 32 (5), 707–722.
- Jiang, W., Wang, L., Feng, L., et al., 2019. Drought characteristics and its impact on changes in surface vegetation from 1981 to 2015 in the Yangtze River Basin, China. *Int. J. Climatol.* 40 (7), 3380–3397.
- Jiang, X.J., Zhu, X., Yuan, Z.Q., Li, X.G., Zakari, S., 2020. Lateral flow between bald and vegetation patches induces the degradation of alpine meadow in qinghai-Tibetan plateau. *Sci. Total Environ.* 751, 142338.
- Jim, Coakley, 2005. Reflections on aerosol cooling. *Nature* 438 (7071), 1091–1092.
- Jing, X., Huang, J., Wang, G., et al., 2010. The effects of clouds and aerosols on net ecosystem CO<sub>2</sub> exchange over semi-arid Loess Plateau of Northwest China. *Atmos. Chem. Phys.* 10 (17), 8205–8218.
- Kato, S., Rose, F.G., Charlock, T.P., 2005. Computation of domain-averaged irradiance using satellite-derived cloud properties. *J. Atmos. Ocean. Technol.* 22, 146–164.
- Krishnan, R., Ramanathan, V., 2002. Evidence of surface cooling from absorbing aerosols. *Geophys. Res. Lett.* 29 (9).
- Lawal, S., Lennard, C., Jack, C., Wolski, P., Abiodun, B., 2019. The observed and model-simulated response of southern African vegetation to drought. *Agric. For. Meteorol.* 279.
- Lawrence, P.J., Chase, T.N., 2007. Representing a MODIS consistent land surface in the Community Land Model (CLM 3.0). *J. Geophys. Res. Atmos.* 112, 1–17.
- Lee, J.J., Neely, G.E., Perrigan, S.C., et al., 1981. Effect of simulated sulfuric acid rain on yield, growth and foliar injury of several crops. *Environ. Exp. Bot.* 21 (2), 171–185.
- Li, G., Fang, C., Wang, S., et al., 2016. The Effect of Economic Growth, Urbanization, and Industrialization on Fine Particulate Matter (PM2.5) Concentrations in China. *Environmental Science & Technology*, p. 11452.
- Li, Z., Lee, K.H., Wang, Y., et al., 2010. First observation-based estimates of cloud-free aerosol radiative forcing across China. *J. Geophys. Res.: Atmosphere* 115, D00K18.
- Lin, L., Fu, Q., Zhang, H., Su, J., Yang, Q., Sun, Z., 2013. Upward mass fluxes in tropical upper troposphere and lower stratosphere derived from radiative transfer calculations. *J. Quant. Spectrosc. Radiat. Transfer* 117, 114–122.
- Mai, B., Deng, X., Li, Z., et al., 2018. Aerosol optical properties and radiative impacts in the Pearl River Delta region of China during the dry season. *Adv. Atmos. Sci.* 35, 195–208.
- Map, M., Cr, T., Lw, T., 1995. Atmospheric effects of the Mt Pinatubo eruption. *Nature* 373 (6513), 399–404.
- Nemani, R.R., Running, S.W., 1996. Implementation of a hierarchical global vegetation classification in ecosystem function models. *J. Veg. Sci.* 7, 337–346.
- Oleson, K.W., Lawrence, D.M., Bonan, G.B., et al., 2013. Technical Description of Version 4.5 of the Community Land Model (CLM). NCAR Technical Note: NCAR/TN-503+STR. National Center for Atmospheric Research (NCAR), Boulder, CO, USA.
- Pastorello, G., Trotta, C., Canfora, E., et al., 2020. The FLUXNET2015 dataset and the ONEflux processing pipeline for eddy covariance data. *Scientific Data* 7 (1), 225–251.
- Qian, W., Quan, L., Shi, S., 2002. Variations of the dust storm in China and its climatic control. *J. Clim.* 15 (10), 1216–1229.
- Qin, W., Liu, Y., Wang, L., et al., 2018. Characteristic and driving factors of aerosol optical depth over mainland China during 1980–2017. *Rem. Sens.* 10 (7), 1064.
- Ramankutty, N., Evan, A.T., Monfreda, C., et al., 2008. Farming the planet: 1. Geographic distribution of global agricultural lands in the year 2000. *Global Biogeochem. Cycles* 22 (1), 1–19.
- Rap, A., Scott, C.E., Reddington, C.L., et al., 2018. Enhanced global primary production by biogenic aerosol via diffuse radiation fertilization. *Nat. Geosci.* 11 (9), 640–647.
- Rose, F., Charlock, T., 2002. New Fu Liou code tested with ARM Raman lidar and CERES in pre CALIPSO exercise. In: Extended Abstract for 11th Conference on Atmospheric Radiation (AMS), Ogden, Utah, vol. 37.
- Shao, L., Li, G., Zhao, Q., et al., 2020. The fertilization effect of global dimming on crop yields is not attributed to an improved light interception. *Global Change Biol.* 26 (3), 1–17.
- Smith, D.M., Booth, B., Dunstone, N.J., Eade, R., Hermanson, L., Jones, G.S., et al., 2016. Role of volcanic and anthropogenic aerosols in the recent global surface warming slowdown. *Nat. Clim. Change* 936–940.
- Still, C.J., Berry, J.A., Collatz, G.J., et al., 2003. Global distribution of C3 and C4 vegetation: carbon cycle implications. *Global Biogeochem. Cycles* 17 (1), 1–14.
- Stocker, T.F., Qin, D., Plattner, G.F., 2013. Climate Change 2013: The Physical Science Basis. Contribution of Working Group I to the Fifth Assessment Report of the Intergovernmental Panel on Climate Change. *Comput. Geom.* 18, 95–123.
- Unger, N., Yue, X., Harper, K.L., 2017. Aerosol climate change effects on land ecosystem services. *Faraday Discuss.* 200, 121–142.
- Vivoni, E.R., 2018. CRUNCEP Version 7 - Atmospheric Forcing Data for the Community Land Model. Research Data Archive at the National Center for Atmospheric Research, Computational and Information Systems Laboratory. <https://doi.org/10.5065/PZ8F-F017>.
- Wei, J., Li, Z., Pinker, R., 2021a. Himawari-8-derived diurnal variations of ground-level PM2.5 pollution across China using the fast space-time Light Gradient Boosting Machine (LightGBM). *Atmospheric Chemistry and Physics* 21, 7863–7880.
- Wei, J., Li, Z., Xue, W., et al., 2021b. The ChinaHighPM10 dataset: generation, validation, and spatiotemporal variations from 2015 to 2019 across China. *Environment International* 146, 106290.
- Xie, X., Wang, T., Yue, X., et al., 2020. Effects of atmospheric aerosols on terrestrial carbon fluxes and CO<sub>2</sub> concentrations in China. *Atmos. Res.* 237, 104859.
- Xu, P., Chen, Y., Ye, X., 2013. Haze, air pollution, and health in China. *Lancet* 382 (9910), 2067.

- Xue, W., Zhang, J., Qiao, Y., et al., 2020a. Spatiotemporal variations and relationships of aerosol-radiation-ecosystem productivity over China during 2001–2014. *Sci. Total Environ.* 741, 140324.
- Xue, W., Zhang, J., Zhong, C., et al., 2020b. Satellite-derived spatiotemporal PM2.5 concentrations and variations from 2006 to 2017 in China. *Sci. Total Environ.* 712, 134577.
- Xue, W., Zhang, J., Zhong, C., et al., 2021. Spatiotemporal PM2.5 variations and its response to the industrial structure from 2000 to 2018 in the Beijing-Tianjin-Hebei region. *J. Clean. Prod.* 27, 123742.
- Yan, X., Shi, W., Zhao, W., et al., 2014. Impact of aerosols and atmospheric particles on plant leaf proteins. *Atmos. Environ.* 88, 115–122.
- Yang, Y., Zhao, C., Wang, Q., Cong, Z., Yang, X., Fan, H., 2021. Aerosol characteristics at the three poles of the earth as characterized by cloud-aerosol lidar and infrared pathfinder satellite observations. *Atmos. Chem. Phys.* 4849–4868. <https://doi.org/10.5194/acp-21-4849-2021>.
- Yu, H., Kaufman, Y.J., Chin, M., Feingold, G., Remer, L.A., Anderson, T.L., et al., 2005. A review of measurement-based assessments of the aerosol direct radiative effect and forcing. *Atmos. Chem. Phys.* 6 (3), 613–666.
- Yue, X., Unger, N., 2018. Fire air pollution reduces global terrestrial productivity. *Nat. Commun.* 9 (1), 1–10.
- Yue, X., Strada, S., Unger, N., et al., 2017a. Future inhibition of ecosystem productivity by increasing wildfire pollution over boreal north America. *Atmos. Chem. Phys.* 17 (22), 13699–13719.
- Yue, X., Unger, N., Harper, K., et al., 2017b. Ozone and haze pollution weakens net primary productivity in China. *Atmos. Chem. Phys.* 17 (9), 6073–6089.
- Zhang, H., Hu, J., Qi, Y., et al., 2017. Emission characterization, environmental impact, and control measure of PM2.5 emitted from agricultural crop residue burning in China. *J. Clean. Prod.* 149, 629–635.
- Zhang, J., Ding, J., Zhang, J., et al., 2020. Effects of increasing aerosol optical depth on the gross primary productivity in China during 2000–2014. *Ecol. Indicat.* 108, 105761.
- Zhang, M., Wang, Y., Ma, Y., et al., 2018. Spatial distribution and temporal variation of aerosol optical depth and radiative effect in South China and its adjacent area. *Atmos. Environ.* 188, 120–128.
- Zhang, Q., He, K., Huo, H., 2012. Policy: cleaning China's air. *Nature* 484 (7393), 161–162.
- Zhang, Y., Goll, D., Bastos, A., et al., 2019. Increased global land carbon sink due to aerosol-induced cooling. *Global Biogeochem. Cycles* 33, 439–457.
- Zhang, Y., Wen, X.Y., Jang, C.J., 2010. Simulating chemistry-aerosol-cloud-radiation-climate feedbacks over the continental U.S. using the online-coupled weather research forecasting model with chemistry (wrf/chem). *Atmos. Environ.* 44 (29), 3568–3582.
- Zheng, S., Pozzer, A., Cao, C.X., et al., 2015. Long-term (2001–2012) concentrations of fine particulate matter (PM2.5) and the impact on human health in Beijing, China. *Atmos. Chem. Phys.* 15, 5715–5725.